



# Reducing Energy Consumption in CubeSat Missions: The Integrated Antenna Approach

Gulama-Garip Alisher E. Ibrayev,<sup>1</sup> Nursultan Meirambekuly,<sup>1,3,\*</sup> Beibit A. Karibayev,<sup>1,2</sup> Timur A. Namazbayev,<sup>1</sup> Sabyrzhan O. Orynassar,<sup>1</sup> Anna S. Sukhenko,<sup>1,4</sup> Amirkhan A. Temirbayev<sup>1,\*</sup> and AlgaZY Zhauyt<sup>2</sup>

## Abstract

One of the future challenges of increasing the harnessed solar power is efficiently using the CubeSat sides. One of the approaches is using integrated antenna systems with solar panels or payloads. This study proposes a new approach to using integrated antenna systems in remote sensing missions. In this approach, due to the integration of the antenna system with payload (in our case, with the camera), it is possible to achieve a significant increase in power generation. Calculations are performed for cases when the antenna system is integrated with the optical system ( $\alpha = 0^\circ$ ), which means that they use the same plane. In the second case, they are separated by an angle of  $\alpha = 90^\circ$ , and in the third case, when they are pointed in opposite directions ( $\alpha = 180^\circ$ ). In the case of  $\alpha = 0^\circ$ , where the camera and antenna module are aligned co-axially, there is no energy expenditure for CubeSat orientation. However, in the other two cases, energy is required for rotation and maintenance of the specified orientation throughout the entire duration of the satellite's flight over the ground station, amounting to 111.99 mW when  $\alpha = 90^\circ$  and 44.33 mW when  $\alpha = 180^\circ$ . This study is significant because it provides a data-driven approach to CubeSat design, emphasizing the importance of camera and antenna alignment in improving operational efficiency. By demonstrating how optimal configurations can lead to faster response times and reduced power consumption, the results can inform future mission planning and improve the overall effectiveness of small satellite operations.

**Keywords:** CubeSat; Integrated antenna systems; Remote sensing; Altitude control; Energy Budget.

Received: 23 July 2024; Revised: 27 October 2024; Accepted: 29 October 2024.

Article type: Research article.

## 1. Introduction

CubeSats have revolutionized space exploration and scientific research due to their low cost, rapid development cycles, and increased accessibility.<sup>[1,2]</sup> These compact, lightweight satellites have opened the door for a surge in space missions, enabling a wide range of applications across various scientific disciplines, from Earth observation to deep space exploration.<sup>[3-6]</sup> According to the world's largest NanoSat

database, from 2000 to May 2023, more than 2,286 nanosatellites (of which 2,105 were CubeSats) weighing less than 10 kg have been successfully launched.<sup>[7]</sup> This remarkable growth highlights the increasing adoption of CubeSat technology across academia, industry, and space agencies. CubeSat nanosatellites play a key role in the development of space research, providing access to space for various scientific tasks at low cost and a fast development cycle.

Despite their popularity and exponential growth, CubeSats still face several limitations.<sup>[8,9]</sup> Their small size and volume constraints make it challenging to accommodate all necessary components, such as electronics, antennas, payloads, and solar panels. Large-volume antennas, in particular, with complex deployable systems, are often excluded from CubeSat designs due to these space limitations. Additionally, CubeSats must carefully balance size, weight, and power (SWaP) considerations, which makes maximizing the spacecraft's efficiency a significant challenge.

<sup>1</sup> Al-Farabi Kazakh National University, Almaty, 050038, Kazakhstan.

<sup>2</sup> Almaty University of Power Engineering and Telecommunications named after Gumarbek Daukeyev, Almaty, 050013, Kazakhstan.

<sup>3</sup> Khoja Akhmet Yassawi International Kazakh-Turkish University, Turkistan, 160400, Kazakhstan.

<sup>4</sup> AALR "Institute of Space Technique and Technology", Almaty, 050061, Kazakhstan.

\*Email: [nursultan.meirambekuly@kaznu.edu.kz](mailto:nursultan.meirambekuly@kaznu.edu.kz) (N.

Meirambekuly), [amirkhant@gmail.com](mailto:amirkhant@gmail.com) (A. A. Temirbayev)

A crucial subsystem of CubeSat missions, particularly in complex missions like Earth observation and remote sensing, is the electrical power supply (EPS).<sup>[9]</sup> The EPS plays a key role in supporting high data transfer rates while maintaining power for various onboard instruments. CubeSats are often deployed in low-Earth orbit (LEO), where power generation is limited due to the small surface area available for solar panels. In such missions, energy conservation is critical, especially when managing power-hungry tasks like data transmission. The challenge of optimizing power usage becomes even more significant when CubeSats are required to operate autonomously for extended periods in space with minimal human intervention. Addressing energy conservation is, therefore, a highly relevant task in CubeSat technology.

One of the critical challenges is increasing the efficiency of power generation while simultaneously reducing energy consumption across all subsystems. Effective utilization of CubeSat surfaces is a key factor, as the limited space must be used for solar panels, antennas, and payloads without compromising performance. A promising approach to address this issue is the integration of antennas with solar panels or payloads. By embedding antennas into the surface area of the CubeSat, it becomes possible to use the same structure for both communication and power generation purposes.<sup>[10-14]</sup> This approach not only saves space by eliminating the need for separate deployable antenna systems but also reduces the overall size and weight of the CubeSat.

Previously, the authors of this study have proposed the integration of patch antennas and spiral antennas on CubeSats, exploring various options for embedding antennas into the CubeSat structure.<sup>[12-14]</sup> However, the advantages of this approach in terms of energy budget optimization have not been fully demonstrated in earlier work. In this paper, we present a novel approach to the utilization of integrated antenna systems for optimizing the energy budget in Earth observation missions. By effectively integrating communication systems with power generation components, this approach seeks to maximize CubeSat's limited resources, ensuring that energy constraints are minimized while maintaining mission performance and data transmission capabilities.

This paper will explore how integrating antennas with solar panels or payload surfaces can enhance the energy efficiency of CubeSats and contribute to the overall success of complex missions. The novel method presented here focuses on Earth observation missions, where high data transfer rates and long-duration operations are critical, making energy optimization a primary concern.

## 2. Materials and methods

The successful execution of Earth observation missions necessitates a high level of precision in orienting the satellite towards the Earth's surface. Practical experience has shown that these challenges can be addressed through the utilization of active and, in some cases, combined altitude control systems, which have the capability to provide the required level of accuracy. At present, small satellites widely employ gyroscopic systems as an active attitude control system.<sup>[15]</sup> These systems manage the spacecraft's angular position by exchanging angular momentum between inertial rotating masses and the spacecraft's body. The adjustment of the gyroscopic system's angular momentum is achieved by regulating the rotation speed of the gyroscopes. Based on their operating principles, gyroscopic systems can be categorized into relay, pulse, and linear gyroscopic systems.<sup>[15-19]</sup> Well-established methods from control theory and optimal control, such as Proportional Integral Derivative (PID), Linear Quadratic Regulator (LQR), Proportional Derivative (PD), Proportional (P), Robust Linear Models (RLM), and others, are employed for the analysis of gyroscopic system dynamics.<sup>[20-22]</sup> These methods are valuable tools for studying and optimizing the performance of gyroscopic systems. There are a number of research dedicated to gyroscopic systems where they are examined from a similar perspective. In these studies, PD controllers are commonly used as the control law, based on error and rate matching, with various methods of motion specification. Quaternion representations are frequently encountered in these studies.<sup>[23,24]</sup> Tsitorias presented several parameterizations of motion relative to the center of mass, along with the corresponding control laws for each parameterization.<sup>[25]</sup> Each set of parameters has its own advantages and disadvantages, and the choice is typically driven by the specific objectives of the mission. However, it is evident that the ultimate results achieved tend to be analogous regardless of the chosen parameterization. The presented work focuses on specifying the orientation using a matrix of direction cosines. An important aspect is the selection of the PD controller coefficients. Ultimately, these coefficients can affect parameters such as the turnaround time, energy consumption, and more. In the current study, the criterion for selecting these parameters is the speed of transient processes. In some works dedicated to gyroscopic system algorithms, the question of parameter selection is either omitted, and only a few algorithm performance examples are provided, or numerical methods are used to determine these parameters.<sup>[26, 27]</sup>

Dynamic Euler's equations were employed to assess the responsiveness of altitude control for the rotation of the

spacecraft relative to the position of the antenna-optical systems. These equations (1-3) can be expressed as follows:<sup>[16-18]</sup>

$$\sum M_x = J_{xx}\dot{\omega}_x - J_{xy}\dot{\omega}_y - J_{xz}\dot{\omega}_z + (J_{zz} - J_{yy})\omega_y\omega_z + J_{yz}(\omega_z^2 - \omega_y^2) + \omega_x(J_{xy}\omega_z - J_{xz}\omega_y) \quad (1)$$

$$\sum M_y = -J_{xy}\dot{\omega}_x + J_{yy}\dot{\omega}_y - J_{yz}\dot{\omega}_z + (J_{xx} - J_{zz})\omega_x\omega_z + J_{xz}(\omega_x^2 - \omega_z^2) + \omega_y(J_{yz}\omega_x - J_{xy}\omega_z) \quad (2)$$

$$\sum M_z = J_{xz}\dot{\omega}_x - J_{yz}\dot{\omega}_y + J_{zz}\dot{\omega}_z + (J_{yy} - J_{xx})\omega_x\omega_y + J_{xy}(\omega_y^2 - \omega_x^2) + \omega_x(J_{xz}\omega_y - J_{yz}\omega_x) \quad (3)$$

For deriving the system of equations, Euler angles (Fig. 1) were utilized, along with transition matrices from the spacecraft-fixed coordinate system  $O_{XYZ}$  to the specified system  $O_{xyz}$  in the form:

$$R_\psi = \begin{bmatrix} 1 & 0 & 0 \\ 0 & \cos \psi & \sin \psi \\ 0 & -\sin \psi & \cos \psi \end{bmatrix}$$

$$R_\theta = \begin{bmatrix} \cos \theta & 0 & -\sin \theta \\ 0 & 1 & 0 \\ \sin \theta & 0 & \cos \theta \end{bmatrix}$$

$$R_\phi = \begin{bmatrix} \cos \phi & \sin \phi & 0 \\ -\sin \phi & \cos \phi & 0 \\ 0 & 0 & 1 \end{bmatrix}$$

$$R_{xx} = R_\psi R_\theta R_\phi = \begin{bmatrix} \cos \phi \cos \theta & \sin \phi \cos \theta & -\sin \theta \\ \cos \phi \sin \theta \sin \psi - \sin \phi \cos \psi & \sin \phi \sin \theta \sin \psi + \cos \phi \cos \psi & \cos \theta \sin \psi \\ \cos \phi \sin \theta \cos \psi + \sin \phi \sin \psi & \sin \phi \sin \theta \cos \psi - \cos \phi \sin \psi & \cos \theta \cos \psi \end{bmatrix} \quad (7)$$

The equations (1-3), concerning the principal moments of inertia, can be simplified through linearization and rewritten in the following form:

$$J_{xx}\dot{\omega}_x + (J_{zz} - J_{yy})\omega_y\omega_z = \sum M_x \quad (8)$$

$$J_{yy}\dot{\omega}_y + (J_{xx} - J_{zz})\omega_x\omega_z = \sum M_y \quad (9)$$

$$J_{zz}\dot{\omega}_z + (J_{yy} - J_{xx})\omega_x\omega_y = \sum M_z \quad (10)$$

$$\dot{\omega}_x = \ddot{\psi} + n\dot{\phi} \quad (11)$$

$$\dot{\omega}_y = \ddot{\theta} \quad (12)$$

$$\dot{\omega}_z = \ddot{\phi} - n\dot{\psi} \quad (13)$$

where  $n = \sqrt{\mu/r_0^3}$  represents the mean motion, with  $\mu$  being the gravitational parameter and  $r_0$  representing the initial radius from the center of mass of the Earth. This parameter is crucial for characterizing the average orbital motion of the

spacecraft.

At the given altitude, the total torque about roll ( $M_x$ ), pitch ( $M_y$ ), and yaw ( $M_z$ ) axes includes a perturbing gravitational torque,<sup>[10]</sup> which can be expressed as follows:

$$M_x = 3n^2(J_{zz} - J_{yy}) \cos \psi \sin \psi \cos^2 \theta = 3n^2(J_{zz} - J_{yy})\psi \quad (14)$$

$$M_y = -3n^2(J_{xx} - J_{zz}) \cos \psi \sin \theta \cos \theta = -3n^2(J_{xx} - J_{zz})\theta \quad (15)$$

$$M_z = -3n^2(J_{yy} - J_{xx}) \sin \psi \sin \theta \cos \theta = 0 \quad (16)$$

Taking into account the presence of gyroscopes, the change in the kinetic moment of the system can be determined as follows:

$$M = \dot{H} = (\dot{H} + \omega \times H) \quad (17)$$

where

$$H = H_G^{body} + H_G^{flywheel-1} + H_G^{flywheel-2} + H_G^{flywheel-3} =$$

$$H_G^{body} + \sum_{i=1}^3 H_G^{flywheel-i} \quad (18)$$

$$H_G^{body} = J^{body}\omega, H_G^{flywheel-i} = J^{flywheel-i}\omega^{(i)}, \omega^{(i)} = \omega + w^{(i)} \quad (19)$$

$$J^{body} = \begin{bmatrix} J_{xx} & 0 & 0 \\ 0 & J_{yy} & 0 \\ 0 & 0 & J_{zz} \end{bmatrix}, J^{flywheel-i} = \begin{bmatrix} J_{xx}^{(i)} & 0 & 0 \\ 0 & J_{yy}^{(i)} & 0 \\ 0 & 0 & J_{zz}^{(i)} \end{bmatrix} \quad (20)$$

where  $\omega$  – the spacecraft angular velocity,  $w^{(i)}$  – relative angular velocity of the  $i$ -th flywheel with respect to the spacecraft.

Taking into account the relationships given in equations (18-20), the system of equation (17) can be rewritten as follows:

$$J\dot{\omega} + \dot{H}_G^{flywheels} + \omega \times (J\omega + H_G^{flywheels}) = M \quad (21)$$

where

$$J = J^{body} + J^{flywheels}, J^{flywheels} = \sum_{i=1}^3 \begin{bmatrix} J_{xx}^{(i)} & 0 & 0 \\ 0 & J_{yy}^{(i)} & 0 \\ 0 & 0 & J_{zz}^{(i)} \end{bmatrix} \quad (22)$$

$$H_G^{flywheels} = \sum_{i=1}^3 \begin{bmatrix} J_{xx}^{(i)} & 0 & 0 \\ 0 & J_{yy}^{(i)} & 0 \\ 0 & 0 & J_{zz}^{(i)} \end{bmatrix} \begin{bmatrix} w_x^{(i)} \\ w_y^{(i)} \\ w_z^{(i)} \end{bmatrix}, w^{(i)} = \begin{bmatrix} w_x^{(i)} \\ w_y^{(i)} \\ w_z^{(i)} \end{bmatrix},$$

$$\omega = \begin{pmatrix} \omega_x \\ \omega_y \\ \omega_z \end{pmatrix} \quad (23)$$

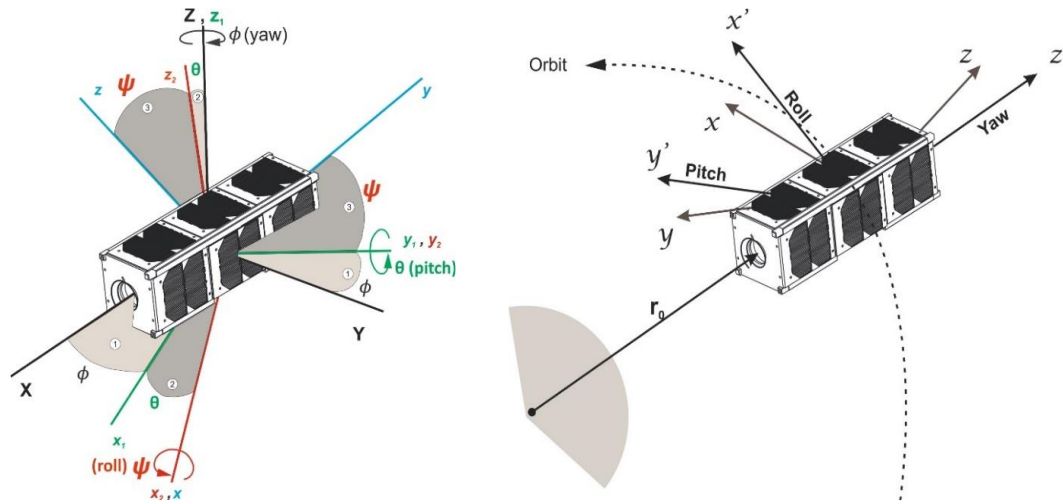


**Fig. 1** Euler angles used for constructing the mathematical model of spacecraft orientation.

Thus, taking into account equations (3)-(5), we obtain a system of linearized equations in the following form:

$$A\ddot{\psi} + \left( n \sum_{i=1}^3 J_{yy}^{(i)} \omega_y^{(i)} - 4n^2(C - B) \right) \psi + n \left( A + C - B - \sum_{i=1}^3 J_{yy}^{(i)} \omega_y^{(i)} \right) \dot{\phi} + \sum_{i=1}^3 J_{zz}^{(i)} \omega_z^{(i)} \dot{\theta} = - \sum_{i=1}^3 \left( n J_{zz}^{(i)} \omega_z^{(i)} + J_{xx}^{(i)} \dot{\omega}_x^{(i)} \right) \quad (24)$$

$$B\ddot{\theta} + 3n^2(A - C)\theta + \sum_{i=1}^3 \left( J_{xx}^{(i)} \omega_x^{(i)} \dot{\phi} - J_{zz}^{(i)} \omega_z^{(i)} \dot{\psi} - n J_{xx}^{(i)} \omega_x^{(i)} \psi - n J_{zz}^{(i)} \omega_z^{(i)} \phi \right) = - \sum_{i=1}^3 J_{yy}^{(i)} \dot{\omega}_y^{(i)} \quad (25)$$

$$C\ddot{\phi} + \left( n \sum_{i=1}^3 J_{yy}^{(i)} \omega_y^{(i)} + n^2(B - A) \right) \phi + \left( n(B - A - C) + \sum_{i=1}^3 J_{yy}^{(i)} \omega_y^{(i)} \right) \dot{\psi} + \sum_{i=1}^3 J_{xx}^{(i)} \omega_x^{(i)} \dot{\theta} = - \sum_{i=1}^3 \left( n J_{xx}^{(i)} \omega_x^{(i)} + J_{zz}^{(i)} \dot{\omega}_z^{(i)} \right) \quad (26)$$

where  $A = J_{xx} + \sum_{i=1}^3 J_{xx}^{(i)}$ ,  $B = J_{yy} + \sum_{i=1}^3 J_{yy}^{(i)}$ ,  $C = J_{zz} + \sum_{i=1}^3 J_{zz}^{(i)}$ .

Transforming equations (24-26) to second-order small terms and assuming the diagonal form of the gyroscopes' inertia tensor, we obtain:

$$A\ddot{\psi} - 4n^2(C - B)\psi + n(A + C - B)\dot{\phi} = -J_{xx}^{(1)} \dot{\omega}_x^{(1)} \quad (27)$$

$$B\ddot{\theta} + 3n^2(A - C)\theta = -J_{yy}^{(2)} \dot{\omega}_y^{(2)} \quad (28)$$

$$C\ddot{\phi} + n^2(B - A)\phi + n(B - A - C)\dot{\psi} = -J_{zz}^{(3)} \dot{\omega}_z^{(3)} \quad (29)$$

where  $A = J_{xx} + J_{xx}^{(1)}$ ,  $B = J_{yy} + J_{yy}^{(1)}$ ,  $C = J_{zz} + J_{zz}^{(1)}$ ,  $M_x^c =$

$-J_{xx}^{(1)} \dot{\omega}_x^{(1)}$ ,  $M_y^c = -J_{yy}^{(1)} \dot{\omega}_y^{(1)}$ ,  $M_z^c = -J_{zz}^{(1)} \dot{\omega}_z^{(1)}$  – the control moments of the gyroscopes, which are aligned with the principal axes of inertia of the spacecraft coinciding with the axes of the body-fixed coordinate system.

Let's consider the case of a CubeSat 3U (unit) form-factor nanosatellite. Assuming that with a uniform distribution of the payload within the satellite's volume, we can approximate  $B \approx A$ . Then, from the motion equations (24-26), we obtain:

$$A\ddot{\psi} - 4n^2(C - B)\psi + nC\dot{\phi} = -J_{xx}^{(1)} \dot{\omega}_x^{(1)} \quad (30)$$

$$B\ddot{\theta} + 3n^2(A - C)\theta = -J_{yy}^{(2)} \dot{\omega}_y^{(2)} \quad (31)$$

$$C\ddot{\phi} - nC\dot{\psi} = -J_{zz}^{(3)} \dot{\omega}_z^{(3)} \quad (32)$$

Let's assume that the control moment generated by the gyroscopes is determined according to a linear law in the form of a PD controller:

$$M_x^c = -k_1^p \psi - k_1^d \dot{\psi} \quad (33)$$

$$M_y^c = -k_2^p \theta - k_2^d \dot{\theta} \quad (34)$$

$$M_z^c = -k_3^p \phi - k_3^d \dot{\phi} \quad (35)$$

To determine the unknown feedback coefficients, let's transform the system of equations (33-35) into the following form:

$$\dot{X} = AX + Bu \quad (36)$$

$$u = -KX \quad (37)$$

$$X = [x_1, \dots, x_6] = [\psi, \theta, \phi, \dot{\psi}, \dot{\theta}, \dot{\phi}] \quad (38)$$

$$\dot{x}_1 = x_4, \dot{x}_2 = x_5, \dot{x}_3 = x_6, \quad (39)$$

$$\dot{x}_3 = 4n^2 \frac{C-B}{A} x_1 - n \frac{C}{A} x_6 + \frac{M_x^c}{A} \quad (40)$$

$$\dot{x}_4 = 3n^2 \frac{C-A}{B} x_2 + \frac{M_y^c}{B} \quad (41)$$

$$\dot{x}_6 = nx_4 + \frac{M_z^c}{c} \tag{42}$$

$$\mathbf{A} = \begin{bmatrix} 0 & 0 & 0 & 1 & 0 & 0 \\ 0 & 0 & 0 & 0 & 1 & 0 \\ 0 & 0 & 0 & 0 & 0 & 1 \\ \left(4n^2 \frac{c-B}{A}\right) & 0 & 0 & 0 & 0 & \left(-n \frac{c}{A}\right) \\ 0 & \left(3n^2 \frac{c-A}{B}\right) & 0 & 0 & 0 & 0 \\ 0 & 0 & 0 & n & 0 & 0 \end{bmatrix} \tag{43}$$

$$\mathbf{B} = \begin{bmatrix} 0 & 0 & 0 \\ 0 & 0 & 0 \\ 0 & 0 & 0 \\ \frac{1}{A} & 0 & 0 \\ 0 & \frac{1}{B} & 0 \\ 0 & 0 & \frac{1}{C} \end{bmatrix} \tag{44}$$

To determine the feedback coefficients  $k_1^p, k_1^d, k_2^p, k_2^d, k_3^p, k_3^d$  that are part of the coefficient matrix  $\mathbf{K}$ , we will derive them based on the minimization of a cost or performance functional:

$$J = \frac{1}{2} \int (\mathbf{X}^T \mathbf{Q} \mathbf{X} + \mathbf{u}^T \mathbf{R} \mathbf{u}) dt \tag{45}$$

Certainly, the matrix  $\mathbf{K}$  is determined as:

$$\mathbf{K} = -\mathbf{R}^{-1} \mathbf{B}^T \mathbf{P} = \begin{bmatrix} k_1^p & 0 & 0 & k_1^d & 0 & 0 \\ 0 & k_2^p & 0 & 0 & k_2^d & 0 \\ 0 & 0 & k_3^p & 0 & 0 & k_3^d \end{bmatrix} \tag{46}$$

where

$$\mathbf{R} = \frac{1}{M_{max}^c} \cdot \text{diag}[1, 1, 1, 1, 1, 1] \tag{47}$$

The maximum control moment  $M_{max}^c$  can also be incorporated as constraints within the optimization problem, ensuring that the control inputs do not exceed safe operational limits. The matrix  $\mathbf{P}$  can be determined by solving the Riccati equation, a common approach in control system design for optimal control.

$$\mathbf{A}^T \mathbf{P} + \mathbf{P} \mathbf{A} - \mathbf{P} \mathbf{B} \mathbf{R}^{-1} \mathbf{B}^T \mathbf{P} + \mathbf{Q} = 0, \tag{48}$$

where

$$\mathbf{Q} = \Delta X \cdot \text{diag}[1, 1, 1, 1, 1, 1], \tag{49}$$

The term  $\Delta X$  represents the maximum allowable angular deviation from the desired angular position during the orientation mode. It is essentially a tolerance or constraint on how far the spacecraft's orientation can deviate from the desired or reference orientation.

$$\mathbf{P}(t) = \begin{bmatrix} k_1^p \psi + k_1^d \dot{\psi} \\ k_2^p \theta + k_2^d \dot{\theta} \\ k_3^p \phi + k_3^d \dot{\phi} \end{bmatrix} \begin{bmatrix} \omega_x \\ \omega_y \\ \omega_z \end{bmatrix}. \tag{50}$$

### 3. Results and discussion

In our case where the antenna module and camera of the CubeSat are integrated ( $\alpha = 0$ ), there is no energy expenditure for CubeSat orientation. This means that when antenna modules are aligned or integrated such that they have the same orientation as the payload (in our case, camera), there is no need to expend energy to control the orientation of the CubeSat. This configuration allows for energy savings during certain operational modes when orientation control is not required.

The separation of the antenna and optical systems necessitates a transition from the data acquisition mode to the data transmission mode. This transition indeed requires additional energy expenditure. When the antenna and optical systems are separate or misaligned, switching between these modes involves several energy-consuming processes, including reorienting the spacecraft, configuring the communication systems, and potentially activating or deactivating specific components. These energy costs should be considered in the overall energy budget and mission planning for the CubeSat to ensure efficient operation and successful data acquisition and transmission. To illustrate the advantages of our approach, we considered several cases of camera and antenna module placement. In the first case, the camera and antenna module are positioned at a 90° angle to each other, meaning the angle between vectors  $\mathbf{a}$  and  $\mathbf{k}$  is  $\alpha = 90^\circ$  (Fig. 2), where  $\mathbf{a}$  is directed along the normal to the plane of the antenna module's base,  $\mathbf{k}$  is directed along the axis of symmetry of the camera module,  $\alpha$  is the angle between vectors  $\mathbf{a}$  and  $\mathbf{k}$  (Fig. 2, case (a) and (b)). In this scenario, the orientation task involves aligning vector  $\mathbf{k}$  with vector  $\mathbf{a}$ .

In the second case, the antenna module and camera are positioned at a 180° angle to each other (Fig. 3 (b)). This configuration implies that the antenna module and camera are located directly opposite each other with a complete reversal in orientation. For clarity, in Fig. 3 (a), our proposed approach is depicted where the antenna module and camera of the CubeSat are integrated. The moments of inertia, control coefficients and initial conditions mentioned in the context of solving equation (32) for the described cases are provided in Table 1.

When the spacecraft rotates about its own spin axis  $\phi$ , the fastest response and subsequent stabilization with respect to the target direction occur when the antenna module and optical system are positioned perpendicularly ( $\alpha = 90^\circ$  and  $\alpha = 90^\circ+$ ), as shown in Fig. 4. Moreover, in the case of  $\alpha = 90^\circ$ , during the first spacecraft rotation, at the 5<sup>th</sup> second, the amplitude reaches -2.99 milliradians, and then at the 25<sup>th</sup> second, it decreases to 0.28 milliradians, followed by stabilization until the second rotation, where amplitude peaks of -2.85

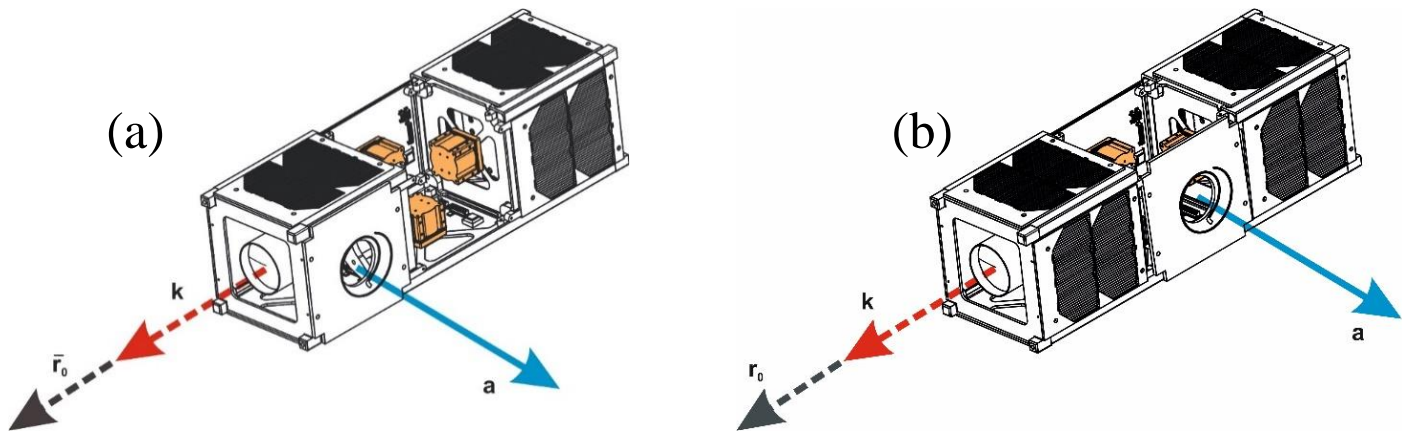


**Fig. 2** The case of placing the antenna module and camera at a 90° angle is further elaborated. (a) the antenna system is offset to the left of the flywheel block and is labeled as “ $\alpha = 90^{\circ+}$ ”, (b) the antenna system is positioned directly above them and is denoted as “ $\alpha = 90^{\circ}$ ”.

**Table 1.** The moments of inertia, control coefficients, and initial conditions.

Case	$\alpha = 0^{\circ}$	$\alpha = 90^{\circ+}$	$\alpha = 90^{\circ}$	$\alpha = 180^{\circ}$
$A, [g, mm^2]$	73964.5	14221	15637.1	14790
$B, [g, mm^2]$	14777.5	14287.3	15733.4	14774.6
$C, [g, mm^2]$	2293.8	2373.4	2497	2293.9
$k_i^p$	0.0000999			
	0.0000997			
	0.0001000			
	0.0316227766015894			
	0.0316227766025173			
$k_i^d$	0.0316227766017297			
	0.0038442			
	0.0017169			
	0.0006774			
	0.0753520120475859			
$\phi(t = 0), [mrad]$			$-\frac{\pi}{4}$	
$\psi(t = 0), [mrad]$			$\frac{\pi}{3}$	
$\theta(t = 0), [mrad]$			$\frac{\pi}{6}$	

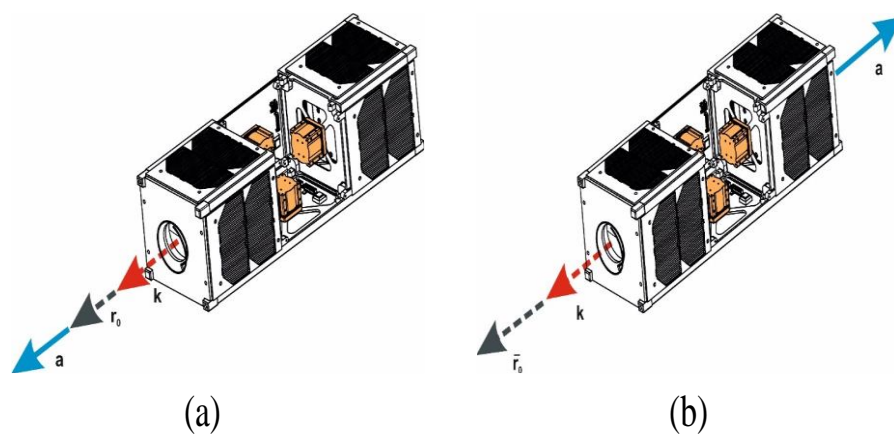


**Fig. 3** The case where the antenna module and camera of the CubeSat are integrated (a) and the case where the antenna module and camera are placed at a 180° angle to each other (b).

milliradians are observed at the 201<sup>st</sup> second and 0.16 milliradians at the 223<sup>rd</sup> second of the flight, followed by further stabilization. Similarly, in the case of  $\alpha = 90^\circ+$ , after the commencement of orientation, an amplitude of -0.78 milliradians is reached at the 22<sup>nd</sup> second, followed by a peak of 0.03 milliradians at the 38<sup>th</sup> second of the flight, with a slight dip observed at the 2.3 milliradians, followed by further stabilization until the second rotation. During the second rotation of this scenario, amplitude peaks of -2.76 milliradians at the 205<sup>th</sup> second and 0.13 milliradians at the 226<sup>th</sup> second are observed, followed by further stabilization. In the case of  $\alpha = 180^\circ$ , after the commencement of orientation with an amplitude of -0.78 milliradians, the following peak at 0.3 milliradians is observed at the 48<sup>th</sup> second, followed by stabilization until the second spacecraft rotation. During the second rotation, several amplitude peaks are observed, specifically, -7.56 milliradians at the 214<sup>th</sup> second, 2.7 milliradians at the 250<sup>th</sup> second, -0.96 milliradians at the 286<sup>th</sup> second, 0.35 milliradians at the 322<sup>nd</sup> second, and -0.12 milliradians at the 358<sup>th</sup> second, followed by further stabilization. These results indicate that the relative positioning of the antenna module and optical system ( $\alpha$ ) has a significant impact not only on the time it takes to achieve orientation but also on the amplitude and phase of the spacecraft's oscillations during the orientation process. The energy consumption analysis provided, according to equation (38), valuable insights into the impact of different  $\alpha$  orientations on energy usage during the CubeSat's mission. For  $\alpha = 90^\circ+$ , the energy consumption is 1.59 mW. In contrast, for  $\alpha = 180^\circ$ , the energy consumption increases to 6.31 mW, which is approximately 3.97 times higher than in the perpendicular case ( $\alpha = 90^\circ+$ ). Indeed, our analysis highlights a crucial point: in cases where the antenna module and optical system are oriented perpendicularly ( $\alpha = 90^\circ+$ ) or in opposite directions ( $\alpha = 180^\circ$ ), additional rotations are required when transitioning from the data acquisition mode to the data transmission mode. These extra rotations can lead to increased energy consumption compared to the scenario where  $\alpha = 0^\circ$ , and the camera and antenna are already aligned.

The observations regarding the orientation response of the CubeSat relative to the nutation angle  $\theta$  provide valuable insights: In the case of  $\alpha = 0^\circ$ , after the commencement of orientation, the spacecraft stabilizes, and practically no other amplitude peaks are observed. This cannot be said for the case of  $\alpha = 90^\circ$ , where after the commencement of orientation with an amplitude of 0.5 milliradians, further amplitude peaks are observed at the 31<sup>st</sup> second with an amplitude of 16.3 milliradians and the 149<sup>th</sup> second with an amplitude of -1.03 milliradians in the first rotation, as well as at the 237<sup>th</sup> second

with an amplitude of 22.7 milliradians, the 329<sup>th</sup> second with an amplitude of -8.25 milliradians, the 422<sup>nd</sup> second with an amplitude of 3 milliradians, and the 525<sup>th</sup> second with an amplitude of -1.09 milliradians in the second rotation, followed by stabilization. In the case of  $\alpha = 90^\circ+$ , after the commencement of orientation, stabilization occurs immediately until the second rotation, where peaks of 21.27 milliradians at the 235<sup>th</sup> second, -7.31 milliradians at the 324<sup>th</sup> second, 2.51 milliradians at the 412<sup>th</sup> second, and -0.87 milliradians at the 501<sup>st</sup> second are observed, followed by further stabilization. In the case of  $\alpha = 180^\circ$ , after the commencement of orientation, stabilization occurs until the second rotation of the spacecraft, where an amplitude peak of 6.82 milliradians is observed at the 213<sup>th</sup> second, followed by further stabilization. This means that the CubeSat can achieve the desired nutation angle relatively quickly in this configuration. However, in the perpendicular case, where the antenna module and optical system are oriented perpendicularly ( $\alpha = 90^\circ+$ ), intense oscillations are observed over a considerably long time interval, extending up to 650 seconds (Fig. 5). This indicates that achieving and stabilizing the desired nutation angle in this configuration takes significantly longer and involves persistent oscillations. The energy consumption and amplitude peaks for different  $\alpha$  configurations ( $\alpha = 180^\circ$ ,  $\alpha = 90^\circ+$ , and  $\alpha = 90^\circ$ ) provide valuable insights into the trade-offs between energy efficiency and nutation control performance: In the case of  $\alpha = 180^\circ$ , the lowest energy consumption is observed, amounting to 11.59 mW. This configuration offers the most energy-efficient nutation control. For  $\alpha = 90^\circ+$  and  $\alpha = 90^\circ$ , the energy consumption values are significantly higher compared to the  $\alpha = 180^\circ$  case. In particular, they are approximately 4.5 times higher than the 180-degree case, with values of 52.7 mW and 57.9 mW, respectively. When calculating the energy consumption, formula (32) was used as before.

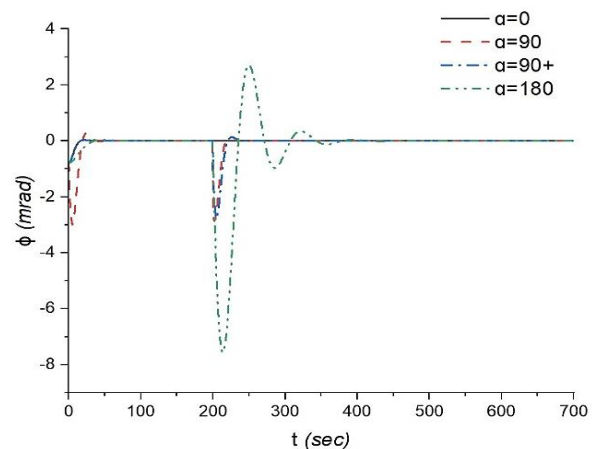


**Fig. 4** The response of the CubeSat's control system when the spacecraft rotates about its own spin axis, represented by the

angle  $\phi$ .

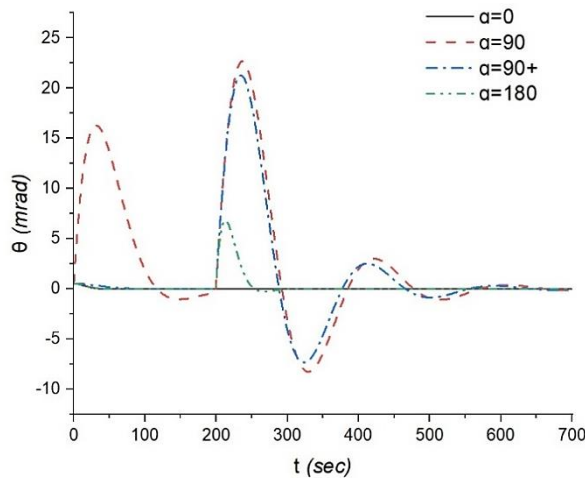


**Fig. 5** The response of the CubeSat's control system when the spacecraft rotates about the nutation angle  $\theta$ .

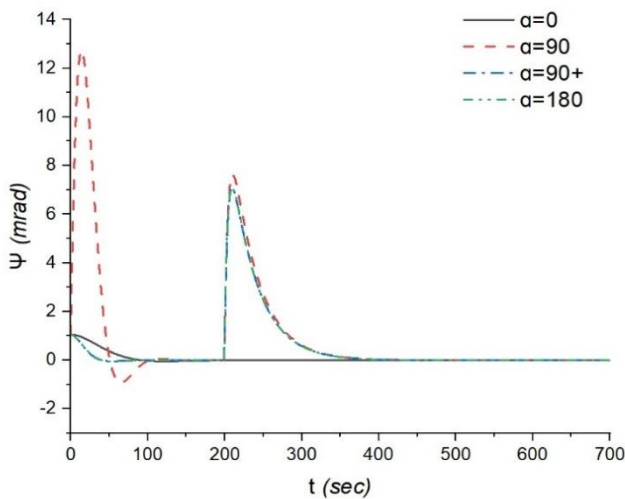


**Fig. 6** The response of the CubeSat's control system when the spacecraft rotates about the precession angle  $\psi$ .

The maximum amplitude peaks for nutation control are as follows: In the case of  $\alpha = 0^\circ$ , after the commencement of spacecraft orientation, stabilization occurs without any other peaks observed (Fig. 6). In the case of  $\alpha = 90^\circ$ , following the initiation of orientation with an amplitude of 1.05 milliradians, peaks are observed with amplitudes of 12.73 milliradians at the 14<sup>th</sup> second and -0.92 milliradians at the 65<sup>th</sup> second during the first rotation, followed by stabilization until the second rotation. In the second rotation, an amplitude peak of 7.62 milliradians is observed at the 62<sup>nd</sup> second, followed by further stabilization. In the case of  $\alpha = 90^\circ+$ , after the commencement of orientation, stabilization occurs until the second rotation, where an amplitude peak of 7.8 milliradians is observed at the 209<sup>th</sup> second, followed by further stabilization. In the case of  $\alpha = 180^\circ$ , a peak is also observed in the second rotation at 7.08 milliradians at the 209<sup>th</sup> second.

The analysis of the response of the CubeSat's control

system during precession ( $\psi$ ) reveals interesting insights: The relative orientation of the antenna module and optical system ( $\alpha$ ) doesn't significantly impact the time and amplitude characteristics of the precession control. Time of Precession: In both cases,  $\alpha = 90^\circ+$  and  $\alpha = 180^\circ$ , the maximum amplitude peak for precession control is reached at 11 seconds, with an amplitude of approximately 7.03 milliradians. Damping of Oscillations: After reaching the maximum amplitude peak, the oscillations dampen relatively quickly, and orientation towards  $\psi$  asymptotically approaches zero. Energy Consumption: In both configurations ( $\alpha = 90^\circ+$  and  $\alpha = 180^\circ$ ), the energy consumption for precession control is 36.9 mW. Antenna Module Position: When the antenna module is placed above the flywheel block, there is a slight increase in amplitude, with a peak amplitude of 7.61 milliradians, still occurring at 11 seconds.

The analysis of energy consumption for orientation control in different  $\alpha$  configurations ( $\alpha = 90^\circ+$ ,  $\alpha = 90^\circ$ , and  $\alpha = 180^\circ$ ) yields important conclusions (Fig. 7). When  $\alpha = 0^\circ$ , the initial power consumption starts at 85 mW, drops to near-minimal levels by the 36<sup>th</sup> second of the flight, and increases to 13 mW and 10 mW at the 51<sup>st</sup> and 93<sup>rd</sup> seconds, respectively, with a near-minimal value at the 73<sup>rd</sup> second. Subsequently, closer to the 140<sup>th</sup> second, the power consumption rises to 2 mW, followed by stabilization at near-minimal levels.

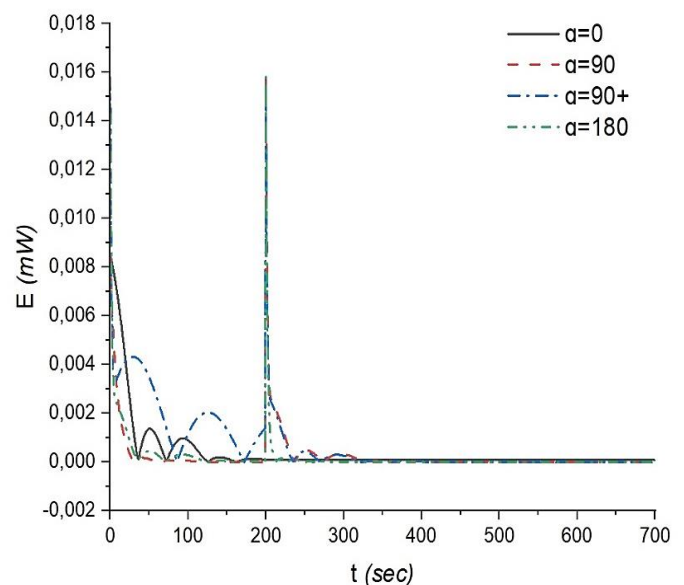


**Fig. 7** The total energy required for rotation and maintaining the desired orientation of the CubeSat.

In the case of  $\alpha = 90^\circ+$ , the power consumption starts at 158 mW, sharply decreases to 32 mW by the 6<sup>th</sup> second, increases to 43 mW by the 29<sup>th</sup> second, drops to near-minimal levels closer to the 86<sup>th</sup> second, and rises to 158 mW at the 200<sup>th</sup> second of the flight, followed by stabilization at near-

minimal levels. The total energy required for rotation and maintaining the desired orientation over the entire duration of the mission when flying over the ground station is 100.73 mW. For  $\alpha = 90^\circ$ , the power consumption starts at 85 mW, decreases, and stabilizes at near-minimal levels by the 50<sup>th</sup> second of the flight. The energy consumption is slightly higher at 111.99 mW. For the  $\alpha = 180^\circ$  configuration, the power consumption, starting at 158 mW, drops to near-minimal levels by the 45<sup>th</sup> second, with slight increases to around 4 mW by the 50<sup>th</sup> and 92<sup>nd</sup> seconds, reaching near-minimal levels between them at the 71<sup>st</sup> second. The power consumption then stabilizes at a near-minimal level. In this case, the energy consumption of the flywheels is significantly lower, totaling 44.33 mW. This represents a 2.27-fold reduction in energy consumption compared to  $\alpha = 90^\circ+$ .

#### 4. Conclusions

This study investigates the advantages of aligning the camera and antenna modules on a CubeSat. The results show that this configuration provides the fastest response time and orientation for the optical system, with minimal amplitudes, and also results in the lowest power consumption.

Key findings and conclusions from the study include:

**Fastest Response in Roll ( $\varphi$ ):** The quickest response and subsequent stabilization relative to the target direction are achieved in perpendicular orientations ( $\alpha = 90^\circ$  and  $\alpha = 90^\circ+$ ), with orientation occurring in 35 seconds.

**Fastest Response in Nutation ( $\theta$ ):** The fastest orientation relative to the target direction is observed at  $\alpha = 180^\circ$ , with orientation occurring in 85 seconds.

**Precession ( $\psi$ ):** The relative angular positioning of the antenna and optical systems does not significantly affect orientation time and oscillation amplitudes. Orientation occurs in 11 seconds.

**Energy Consumption:** The total energy consumption for rotation and maintaining orientation over the mission duration was evaluated for different  $\alpha$  configurations. The results indicate that the  $\alpha = 180^\circ$  configuration has significantly lower energy consumption (44.33 mW) compared to  $\alpha = 90^\circ+$  (100.73 mW) and  $\alpha = 90^\circ$  (111.99 mW). That represents a 2.27-fold reduction in energy consumption compared to  $\alpha = 90^\circ+$ . Overall, the study suggests that aligning the camera and antenna module in a coaxial configuration ( $\alpha = 180^\circ$ ) offers several advantages, including faster response times, minimal oscillation amplitudes, and reduced energy consumption. This makes it a favorable choice for CubeSat orientation control. The findings contribute valuable insights for mission planning and design considerations.

#### Acknowledgments

This research has been funded by the Science Committee of the Ministry of Science and Higher Education of the Republic of Kazakhstan Grant No. AP23488357 “Development and creation of S, X-band antenna arrays integrated with payloads of a small spacecraft of the CubeSat format”.

#### Conflict of Interest

There is no conflict of interest.

#### Open Access

This is an open access article under the CC BY-NC-ND license (<http://creativecommons.org/licenses/by-nc-nd/4.0/>) or CC BY license (<https://creativecommons.org/licenses/by/4.0/deed.en>).

#### Supporting Information

Not applicable.

#### References

- [1] J. Bouwmeester, J. Guo, Survey of worldwide pico- and nanosatellite missions, distributions and subsystem technology, *Acta Astronautica*, 2010, **67**, 854-862, doi: 10.1016/j.actaastro.2010.06.004.
- [2] N. Saeed, A. Elzanaty, H. Almorad, H. Dahrouj, T. Y. Al-Naffouri, M.-S. Alouini, CubeSat communications: recent advances and future challenges, *IEEE Communications Surveys & Tutorials*, 2020, **22**, 1839-1862, doi: 10.1109/COMST.2020.2990499.
- [3] A. Poghosyan, A. Golkar, CubeSat evolution: Analyzing CubeSat capabilities for conducting science missions, *Progress in Aerospace Sciences*, 2017, **88**, 59-83, doi: 10.1016/j.paerosci.2016.11.002.
- [4] C. Cappelletti, D. Robson, CubeSat missions and applications, 2021.
- [5] G. Benedetti, N. Bloise, D. Boi, F. Caruso, A. Civita, S. Corpino, E. Garofalo, G. Governale, L. Mascolo, G. Mazzella, M. Quarata, D. Riccobono, G. Sacchiero, D. Teodonio, P. M. Vernicari, Interplanetary CubeSats for asteroid exploration: mission analysis and design, *Acta Astronautica*, 2019, **154**, 238-255, doi: 10.1016/j.actaastro.2018.05.011.
- [6] F. Davoli, C. Kourogiorgas, M. Marchese, A. Panagopoulos, F. Patrone, Small satellites and CubeSats: survey of structures, architectures, and protocols, *International Journal of Satellite Communications and Networking*, 2019, **37**, 343-359, doi: 10.1002/sat.1277.
- [7] E. Kulu, CubeSats & Nanosatellites-2024 statistics, forecast and reliability, 2024.
- [8] G. Nagel, E. Novo de M, M. Kampel, Nanosatellites applied to optical Earth observation: a review, *Revista Ambiente & Água*, 2020, **15**, e2513, doi:10.4136/ambi-agua.2513.
- [9] S. Liu, P. I. Theoharis, R. Raad, F. Tubbal, A. Theoharis, S. Iranmanesh, S. Abulgasem, M. U. Ali Khan, L. Matekovits, A survey on CubeSat missions and their antenna designs, *Electronics*, 2022, **11**, 2021, doi:

- 10.3390/electronics11132021.
- [10] D. Kim, M. Hwang, G. Kim, S. Kim, Self-deployable circularly polarized phased yagi-uda antenna array using 3-D printing technology for CubeSat applications, *IEEE Antennas and Wireless Propagation Letters*, 2022, **21**, 2249-2253, doi: 10.1109/LAWP.2022.3197359.
- [11] T. R. Jones, J. P. Grey, M. Daneshmand, Solar panel integrated circular polarized aperture-coupled patch antenna for CubeSat applications, *IEEE Antennas and Wireless Propagation Letters*, 2018, **17**, 1895-1899, doi: 10.1109/LAWP.2018.2869321.
- [12] N. Meirambekuly, A. A. Temirbayev, Z. Z. Zhanabaev, B. A. Karibayev, T. A. Namazbayev, B. A. Khaniyev, A. K. Khaniyeva, Dual-band optical imaging system-integrated patch antenna based on anisotropic fractal for earth-observation CubeSats, *Ain Shams Engineering Journal*, 2022, **13**, 101560, doi: 10.1016/j.asej.2021.07.010.
- [13] N. Meirambekuly, B. A. Karibayev, T. A. Namazbayev, G.-G. A. E. Ibrayev, S. O. Orynbassar, S. A. Ivanovich, A. A. Temirbayev, A high gain deployable L/S band conical helix antenna integrated with optical system for earth observation CubeSats, *IEEE Access*, 2023, **11**, 23097-23106, doi: 10.1109/ACCESS.2023.3253556.
- [14] B. Karibayev, N. Meirambekuly, T. Namazbayev, A. Temirbayev, E. Kadylbekkyzy, A. Yessentaeva, S band TT&C antennas integrated with optical camera system for nanosatellites, 2022 International Conference on Electrical, Computer and Energy Technologies (ICECET). Prague, Czech Republic. IEEE, 2022.
- [15] A. V. Sorokin, V. V. Yaremenko, Control moment gyroscopes for spacecraft attitude control systems: history of development, *Gyroscope and Navigation*, 2022, **13**, 53-58, doi: 10.1134/S2075108722010060.
- [16] A. H. De Ruiter, C. Damaren, J. R. Forbes, Spacecraft dynamics and control: an introduction, 2012.
- [17] L. He, W. Ma, P. Guo, T. Sheng, Developments of attitude determination and control system of microsats: A survey, *Journal of Systems and Control Engineering*, 2021, **235**, 1733-1750, doi:10.1177/0959651819895173.
- [18] S. Keshtkar, J. A. Moreno, H. Kojima, K. Uchiyama, M. Nohmi, K. Takaya, Spherical gyroscopic moment stabilizer for attitude control of microsattellites, *Acta Astronautica*, 2018, **143**, 9-15, doi: 10.1016/j.actaastro.2017.10.033.
- [19] V. J. Lappas, W. H. Steyn, C. I. Underwood, Attitude control for small satellites using control moment gyros, *Acta Astronautica*, 2002, **51**, 101-111, doi: 10.1016/S0094-5765(02)00089-9.
- [20] Y. Shiyong, A. Ali, S. Rao, S. Fahad, W. Jing, J. Tong, M. Tahir, Active attitude control for microspacecraft; A survey and new embedded designs, *Advances in Space Research*, 2022, **69**, 3741-3769, doi: 10.1016/j.asr.2022.02.020.
- [21] M. L. Orozco, B. S. Giraldo, Attitude determination and control in small satellites: a review, *IEEE Journal on Miniaturization for Air and Space Systems*, 2024, **5**, 182-186, doi: 10.1109/JMASS.2024.3402984.
- [22] S. N. Norman, Control systems engineering, 2020.
- [23] B. Wie, J. Lu, Feedback control logic for spacecraft eigenaxis rotations under slew rate and control constraints, *Journal of Guidance, Control, and Dynamics*, 1995, **18**, 1372-1379, doi: 10.2514/3.21555.
- [24] B. Wie, P. M. Barba, Quaternion feedback for spacecraft large angle maneuvers, *Journal of Guidance, Control, and Dynamics*, 1985, **8**, 360-365, doi: 10.2514/3.19988.
- [25] A. Mohammadi, E. Rezapour, M. Maggiore, K. Y. Pettersen, Maneuvering control of planar snake robots using virtual holonomic constraints, *IEEE Transactions on Control Systems Technology*, 2015, **24**, 884-899, doi: 10.1109/TCST.2015.2467208.
- [26] S. Kim, Y. Kim, Spin-axis stabilization of a rigid spacecraft using two reaction wheels, *Journal of Guidance, Control, and Dynamics*, 2001, **24**, 1046-1049, doi: 10.2514/2.4818.
- [27] Z. Ismail, R. Varatharajoo, A study of reaction wheel configurations for a 3-axis satellite attitude control, *Advances in Space Research*, 2010, **45**, 750-759, doi: 10.1016/j.asr.2009.11.004.

**Publisher's Note:** Engineered Science Publisher remains neutral with regard to jurisdictional claims in published maps and institutional affiliations.